Spectra of secondary electrons induced by channeled and nonchanneled ions in Si and Al

P. F. A. Alkemade,[1] L. Flinn,[2] W. N. Lennard,[2] and I. V. Mitchell[2]
[1]*Delft Institute of MicroElectronics and Submicron Technology, Faculty of Applied Physics, Delft University of Technology, Lorentzweg 1, 2628 CJ Delft, The Netherlands*
[2]*Interface Science Western, Department of Physics, The University of Western Ontario, London, Ontario, Canada N6A 3K7*
(Received 20 June 1995)

Energy spectra are measured in the (1–2)-keV range of secondary electrons induced by bombardment of Si(100) and Al(110) with a 1.5-MeV He^+ beam. The ion beam is either aligned with a major crystallographic direction or incident along a random direction. The shape of the experimental secondary electron spectra are successfully compared with that of spectra calculated with an efficient Monte Carlo model for electron-transport simulation. In addition, the effective layer thickness L for secondary electron generation under channeling incidence conditions is determined. It is found that L_A for KLL Auger electron generation is equal to the surface peak area in the spectra of the backscattered ions. This similarity is a consequence of the small values of the backscattering collision diameter and the adiabatic radius for K-shell ionization, as compared to the atomic vibration amplitude. In contrast, L_B for the generation of electrons by direct Coulomb ionization is much larger than that for Auger emission. The large value for L_B—an indication of a reduced channeling effect—is attributed to the relatively large contribution from the moderately localized L shell to the measured spectra.

PACS number(s): 79.20.Rf, 61.85.+p, 32.80.Hd, 34.50.Dy

I. INTRODUCTION

A number of techniques for surface or thin layer analysis rely on the detection of emitted or reflected electrons, e.g., x-ray photoemission spectroscopy (XPS), Auger electron spectroscopy (AES), and scanning electron microscopy (SEM) [1]. The measured signal (i.e., intensity of the electrons of a particular energy and direction) depends strongly on elastic and inelastic scattering of the electrons within the solid. However, the relationship between the scattering processes and the signal intensity is so complex as to restrict these analytical techniques. It is mainly for this reason that quite a number of analytical (e.g., [2–6]) or Monte Carlo models (e.g., [7–15]) for the transport of electrons in solids have been developed.

Wong *et al.* [16] and Alkemade and co-workers [17,18] demonstrated that ion-induced Auger electron spectroscopy (IIAES) in combination with ion channeling could also be used to study the transport of energetic electrons in solids. It was argued that it is easier to study electron transport using *ion-induced* rather than *electron-induced* secondary electron emission because effects of the primary and secondary beams can be treated separately. For instance, if the specimen studied is a single crystal, one can influence the depth dependence of the emission rate by ion channeling. Several years ago, MacDonald *et al.* [19,20] studied the effect of ion channeling on IIAES. The authors successfully explained the observed differences in random and aligned Si (KLL), Ni (LMM), and Au (MNN) Auger signal intensities measured in the energy-differential mode. They used a model that included the shadow cone radius, the atomic vibration amplitude, the adiabatic radius for inner-shell ionization, and the Auger electron escape depth. In fact, MacDonald and co-workers suggested that IIAES in combination with ion channeling could possibly be used for structural analysis, e.g., location of a low-Z element in a high-Z single crystal. This application is an alternative for high-energy ion scattering spectroscopy (ISS), which has a poor sensitivity for the example given. The effect of channeling of high-energy ions (E_p/M_1>4 MeV/u) on secondary electron emission has been studied by Kudo *et al.* [21,22]. At energies below the binary-encounter energy, they observed a reduction in spectrum intensities by a factor of 2 to 3.

In Refs. [16,18], we have analyzed energy spectra—measured in the direct, or *nondifferential*, mode—of KLL Auger electrons emitted from Al and Si single crystals under bombardment by ~1-MeV He^+ or H^+ ions. In the analysis a simplified version of the analytical model for electron transport by Tougaard and Sigmund [2] was used. The results, however, were inconclusive: the cross section for elastic scattering appeared to be about an order of magnitude larger than theoretically expected. It was therefore concluded that the analytical approach was oversimplified and that Monte Carlo simulations might prove to be more successful. In Refs. [23–25] a highly efficient Monte Carlo method was introduced that led to a considerable reduction in computation time. High efficiency is achieved by transformations of simulated electron trajectories. Simulated IIAES spectra were obtained that reproduced the experimental Si KLL Auger spectra of Ref. [18] surprisingly well. Moreover, it was tentatively shown that the odd results of the analytical approach were caused by the relatively infrequent inelastic scattering events that involved a large energy loss.

In the present work the efficient Monte Carlo model is applied to simulate spectra of secondary electrons (both KLL Auger and background electrons) emitted from Si or Al single crystals under bombardment by 1.5-MeV He^+ ions. The simulated spectra are compared to spectra measured in the range between 1 and 2 keV, i.e., the range above the binary-encounter energy E_B. A complication in the analysis of the secondary electron spectra is the separation of the Auger contribution and the contribution by direct Coulomb

1050-2947/96/53(2)/886(9)/$06.00 © 1996 The American Physical Society

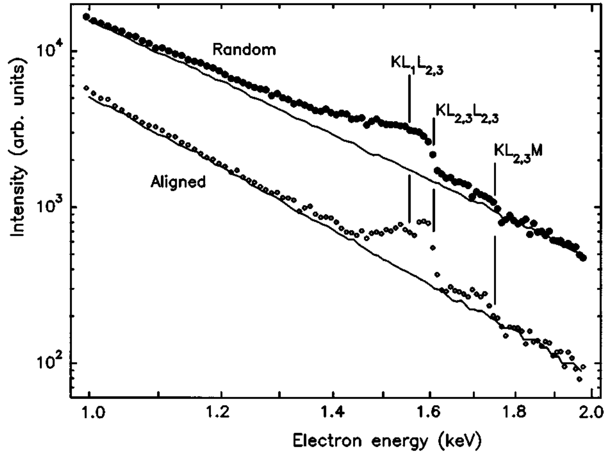

FIG. 1. Secondary electron spectra for Si(100) induced by non-channeled (●) and channeled (○) 1.5-MeV He^+ ions. Full curves are fitted simulated spectra of the background electrons, emitted by direct Coulomb ionization. The various Auger transition energies are indicated.

ionization; the latter is regarded as the background spectrum. With regard to this, we will demonstrate the powerful combination of high-energy ion channeling techniques, secondary electron spectroscopy, and Monte Carlo simulations for a detailed study of secondary electron generation and transport mechanisms.

II. EXPERIMENTS

The experiments were performed in a UHV chamber connected to the 2.5-MV Van de Graaff accelerator at the University of Western Ontario. The chamber was equipped with an argon sputter gun for surface cleaning, a surface barrier particle detector for the detection of backscattered projectiles, an electron gun, and a VG-CLAM hemispherical electron analyzer with an acceptance angle of ~10°. The analyzer was located at an angle of 90° with respect to the ion-beam line, ~10° above the horizontal plane through that line. The specimen was mounted vertically on a five-axis goniometer and heated by a filament at the back side. The rotation axes are the vertical axis and the axis that coincides with the surface normal of the specimen. The former defines the polar angle; the latter, the azimuthal angle. The Al(110) surface was cleaned by repeated cycles of Ar ion sputtering and annealing; the Si(100) surface, by resistive heating at ~1300 K. The cleanliness of the surface was checked by electron-induced AES.

TABLE I. Measured ratios between aligned (Y^a) and random secondary electron spectrum intensities (Y^r), and minimal yield (χ_{min}) of ion backscattering. Background (B) and Auger (A) intensities are evaluated at the main Auger transition energy.

Crystal	Incidence direction	Y^a_B/Y^r_B (%)	Y^a_A/Y^r_A (%)	χ_{min} (%)
Si(100)	[110]	21±2	36±5	3
Al(110)	[011]	30±2	39±5	6
Al(110)	[010]	42±2	61±7	6
Al(110)	[111]	57±3	77±8	11

In the channeling measurements, the incident 1.5-MeV He^+ beam was aligned with a major crystallographic direction: [110] for the experiment with Si(100); and [011], [010], or [111] for the experiment with Al(110). For each channeling measurement, a corresponding random measurement was made at the same polar angle but at a continuously varying azimuthal angle. Backscattered ions and secondary electrons in the (0.85–2.0)-keV energy range were collected simultaneously. The energy resolution of the electron analyzer was 12 eV [full width at half maximum (FWHM)]. The measured electron spectra were corrected for the energy dependence of the transmission function of the analyzer and the sensitivity of the channeltron. The estimated maximum error in the correction amounted to ±25%. More details about the equipment can be found in Refs. [16–18,23].

Figure 1 shows two secondary electron spectra for the case of 1.5-MeV He^+ ions on Si(100). For $E<1.6$ keV, the KLL Auger peak is visible, superposed on a background of electrons emitted by direct Coulomb ionization. The full curves are simulated background spectra, discussed in the next section. The upper spectrum is measured under random incidence conditions; the lower one, under aligned conditions. The aligned spectrum is appreciably less intense than the random one; e.g., at 1.2 keV the intensity is only one-quarter of that in the random spectrum (see also Table I). The secondary electron spectra of Al bombarded by 1.5-MeV He^+ ions [16] are qualitatively similar to those of Si. The minimum backscattering yields χ_{min} and the areas of the surface peak (here called the *effective layer thickness* L_{ISS}) in the corresponding ion backscattering spectra are summarized

TABLE II. Effective layer thickness in Å for background secondary electron generation (L_B), KLL Auger electron generation (L_A), and ion backscattering (L_{ISS}), all under channeling incidence conditions.

		Experiment				Theory	
		Secondary electrons			Ions	Electrons	Ions
Crystal	Incidence direction	L_B [a]	L_B [b]	L_A	L_{ISS}	L_K	L_{ISS}
Si(100)	[110]	34±2	33±3	23±3	(32)[c]	22±2	21±2
Al(110)	[011]	36±2	38±4	19±3	17±2	16±2	15±2
Al(110)	[010]	43±3	48±4	30±4	20±3	24±2	23±2
Al(110)	[111]	64±4	57±5	43±6	31±4	36±3	34±3

[a]Via SL-CSDA analysis.
[b]Via Monte Carlo analysis.
[c]Indirectly determined.

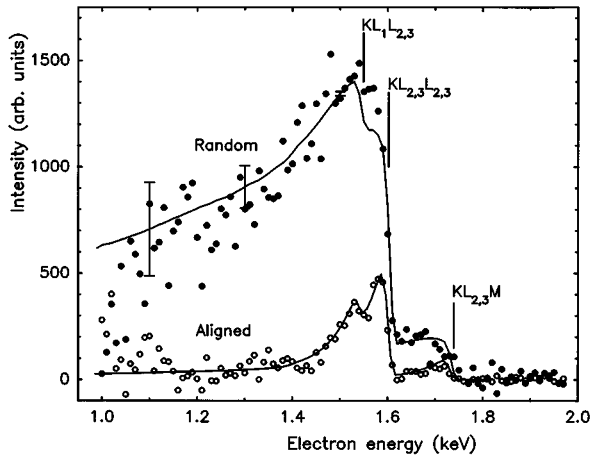

FIG. 2. Residual Si *KLL* and *KLM* Auger electron spectra. Full curves are fitted simulation results. The error bars at 1.1, 1.3, and 1.5 keV indicate the uncertainty arising from the background subtraction procedure.

in Tables I and II. The surface peak area is calculated by comparison with a bismuth-implanted silicon standard [26].

After subtraction of the simulated background from the secondary electron spectra, the spectra of the Auger electrons are obtained. They are shown in Fig. 2 for Si and in Fig. 3 for Al. All Auger spectra measured under *random* incidence conditions are similar. Starting at the higher energy end, we see three steps at the various Auger transitions energies (for Si $KL_{2,3}M$, $KL_{2,3}L_{2,3}$, and $KL_1L_{2,3}$ at 1750, 1617, and 1558 eV, respectively; and for Al at 1487, 1396, and 1345 eV, respectively [27]). Below each step, the Auger spectrum intensity decays slowly with decreasing electron energy. In all random measurements it reaches a level of half the maximum intensity at about 350 eV below the main Auger transition energy. The Auger electron spectra measured under *channeling* incidence conditions are markedly different-: The maximum intensity is 25–65 % lower. Furthermore, the intensity decreases much faster with decreasing electron energy. Half maximum intensity is reached within 100 eV. The largest difference is observed for the most open crystallographic direction, the [011] direction; the smallest difference is observed for the densest direction, [111]. The observed differences between the aligned and random spectra are, of course, related to the differences in the regions where the detected Auger electrons are generated: mainly in the surface region (the outermost few tens of angstroms) for the aligned case and throughout the "whole" solid (the outermost hundreds of angstroms) for the random case. We note that the penetration depth of the ions is much larger than that of the electrons.

III. SHAPE OF THE SECONDARY ELECTRON SPECTRA

Two factors determine the shape of the secondary electron spectra: first, the energy transfer to the secondary electron during the ionization process and, second, the energy loss suffered by the secondary electron while it travels within the solid. For electrons generated by direct Coulomb ionization, the energy-transfer distribution is continuous, but it drops rapidly to zero for energies above the classical limit E_B for

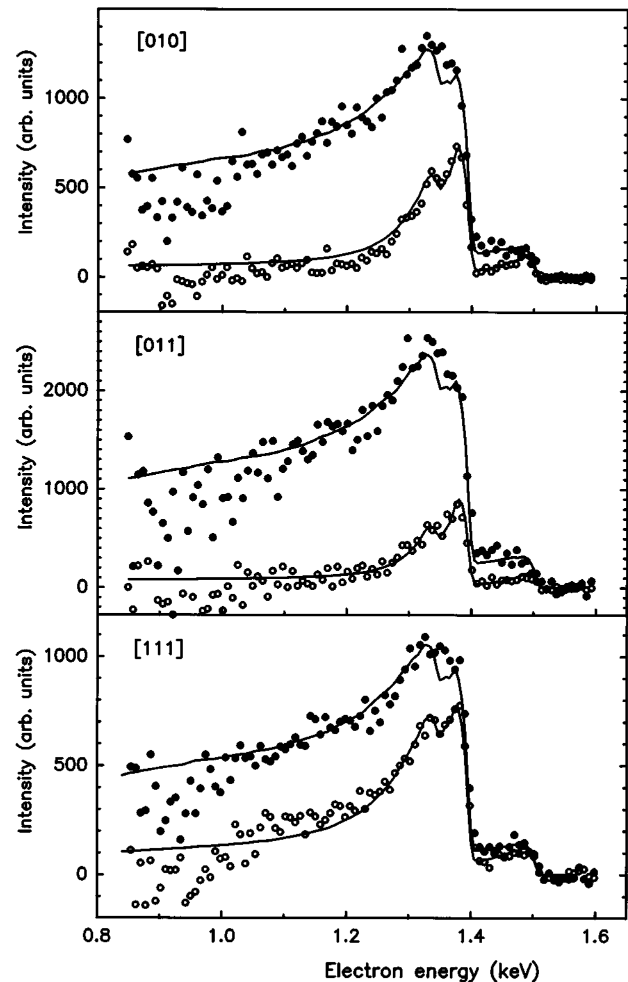

FIG. 3. Residual Al *KLL* and *KLM* Auger electron spectra for various directions of incidence for nonchanneled (●) and channeled (○) ions. Beam doses are 185, 245, and 150 μC for [011], [010], and [111], respectively. Full curves are fitted simulated spectra.

energy transfer to a free electron at rest. ($E_B = 4E_p m_e / M_1$, in which M_1 is the mass of the projectile, E_p its kinetic energy, and m_e the electron mass. For 1.5-MeV He^+ ions, it is 0.81 keV. E_B is called the binary-encounter energy.) These direct ionization electrons cause the continuous background in the secondary electron spectra. In contrast, the energy transfer to an Auger electron is determined by the atomic levels involved in the Auger transition, which implies a discrete distribution. However, in a close encounter collision between an energetic ion and an atom in which a *K*-shell electron is ejected, there is a large probability (>50%) that one or more *L*-shell electrons are ejected simultaneously [28,29]. Such a multiple *KL* or *KM* ionization process affects the levels from which emission occurs and, thus, the energy of the generated *KLL* or *KLM* Auger electrons. Consequently, the inner-shell Auger electron spectra are broadened and shifted. Although some experimental data exist [30,31], no general and quantitative models for these shifts and broadenings are available.

The second factor that determines the shape of the secondary electron spectra is the energy loss of the electrons within the solid. Energy loss is a stochastic process, depend-

ing on several factors, including the path length traveled. The path length of a detected secondary electron depends on the depth and the direction of generation and on deflection by elastic scattering. If the depth of generation is less than the transport mean free path for elastic scattering λ_t [$\lambda_t^{-1} \equiv N \int \sigma_e(\theta)(1-\cos\theta) d\Omega$, in which N is the atomic density and $\sigma_e(\theta)$ is the differential cross section for elastic scattering over an angle θ], then most detected electrons have traveled along straight lines and their path length is proportional to the generation depth [2,18]. On the other hand, if the generation depth is considerably larger than λ_t, most detected electrons have been scattered one or several times before they reach the surface. The transport of these electrons resembles a diffusion process, for which the average path length increases sharply—more or less quadratically—with generation depth [2,18]. Because of the complexity of the electron-transport process, a quantitative analysis of measured spectra must rely on either elaborate analytical or Monte Carlo models. In this work we follow the second approach. Elastic scattering and the discrete and stochastic character of the energy losses are incorporated in our Monte Carlo model [23,25]. Given an initial energy distribution of the generated electrons and a distribution for the depth of generation, the model calculates the energy distribution of the electrons escaping into the vacuum. The local-density approximation by Tung, Ashley, and Ritchie [32] of the dielectric-response model [33] is used for the calculation of the energy-loss distribution. Quantum-mechanical phase-shift cross sections [34–36] are used for the calculation of the deflection angle distribution. The energy dependence of these functions is taken into account. In the simulation model, the medium is assumed to be amorphous; thus, the effect of the crystalline structure of the solid on the angular distribution of emitted secondary electrons is neglected.

A. Approximate analytical model

It is instructive to first apply an approximate model before we discuss the results of the Monte Carlo simulations. In this model we assume that the continuous-slowing-down approximation (CSDA) is applicable and that electrons travel along straight lines; thus elastic scattering is neglected. Then, $\Delta E = Sz/\cos\psi$ (ΔE is the energy loss before escape, S is the stopping power of the medium, z is the generation depth, and ψ is the detection angle with respect to the surface normal). Furthermore, it is assumed that S does not change during electron slow-down. In this straight-line–continuous-slowing-down (SL-CSDA) model, the spectrum height $Y(E)$ can be expressed as

$$Y(E) = k \int_0^\infty r(z) f(E + Sz/\cos\psi) dz, \quad (1)$$

where k is a constant, $r(z)$ is the relative emission rate (equal to the relative number of secondary electrons generated at depth z), and $f(E)$ is the initial energy distribution of the generated electrons. Under random incidence conditions and neglecting any energy loss of the ions, $r(z) = 1$ for all values of z. If the initial energy distribution of the background electrons can be described by a power-law function [37]

$$f(E) = cE^\gamma \quad (\text{with } \gamma < -1), \quad (2)$$

then one finds for the random background height $Y_B^r(E)$

$$Y_B^r(E) = k \int_0^\infty c(E + Sz/\cos\psi)^\gamma dz = \frac{kc(\cos\psi)E^{\gamma+1}}{-(\gamma+1)S} \propto E^{\alpha_r}, \quad (3)$$

with $\alpha_r = \gamma + 1$. Assuming that the background electrons in the aligned case are only generated in a thin surface layer of thickness L_B such that $SL_B/\cos\psi \ll -E/\gamma$, we find for the aligned background height $Y_B^a(E)$

$$Y_B^a(E) = L_B kcE^\gamma \propto E^{\alpha_a}, \quad (4)$$

with $\alpha_a = \gamma$. Thus, the exponent in the aligned spectrum α_a is the same as that in the initial energy distribution, while in the random spectrum it (α_r) differs by $+1$. By combining Eqs. (3) and (4), one gets a simple expression for the effective thickness L_B of the layer in which the background electrons are generated under channeling incidence conditions, expressed in known measurable quantities:

$$L_B = \frac{E \cos\psi}{-(\gamma+1)S} \frac{Y_B^a(E)}{Y_B^r(E)}. \quad (5)$$

From the measured intensity ratios for the background (Table I), the SL-CSDA values for L_B are calculated. These results are shown in the third column of Table II. In principle, one can derive a comparable expression for the Auger electrons. However, such an expression cannot be applied since the CSDA is not valid for Auger emission. This point will be elaborated further in the discussion, viz., Sec. IV B.

B. Monte Carlo simulations of the background spectra

Electrons generated by direct Coulomb ionization form the continuous background in the measured secondary electron spectra. In addition, Auger electrons are detected at all energies below the Auger transition energy E_A [$\approx E_K - 2E_L$ for a KLL Auger electron; E_K (E_L) is the binding energy for a K (L)-shell electron]. It is therefore difficult to separate the continuous but nonconstant background from the Auger spectrum. This is especially true for random incidence conditions, where the Auger contribution remains finite at relatively low energies. Nevertheless, accurate spectrum separation is possible not only for the aligned but also for the random spectra. This will be shown below.

The generation of Si or Al KLL and KLM Auger electrons in the bulk is strongly reduced when the ions are channeled. Then most detected Auger electrons have been generated in the near-surface region ($z < 100$ Å) and thus have suffered energy losses of, in total, at most 200 eV ($\sim S \times 100$ Å). The aligned spectrum in Fig. 1 outside the range between 1.35 and 1.75 keV can therefore be attributed almost exclusively to background electrons. Note that the background electrons are also mainly generated in the near-surface region. We will use the aligned secondary electron spectrum—which resembles the initial energy distribution; see Eq. (4)—and the Monte Carlo model to obtain a reliable estimate for the shape of the (aligned and random) background spectra.

TABLE III. Exponents in the power-law relation between background intensity and energy. α_r, random spectrum; α_a, aligned spectrum; γ, initial energy distribution. The statistical error in all numbers is 0.2; the systematic error is 0.5.

Crystal	Incidence direction	α_r	α_a	γ
Si(100)	[110]	−5.1	−6.0	−6.3
Al(110)	[011]	−5.3	−6.3	−6.5
Al(110)	[010]	−5.1	−5.5	−6.3
Al(110)	[111]	−5.1	−5.7	−6.3

The model calculations need as input parameters the initial energy distribution and the generation-depth distribution of the background electrons. We assume that the power-law function, i.e., Eq. (2), is a good approximation for the initial energy distribution. In the Monte Carlo simulations, the parameters γ and c of Eq. (2) are varied until good agreement is obtained between the simulated and measured aligned secondary electron spectra outside the Si Auger region between 1.35 and 1.75 keV. For the generation-depth distribution under channeling incidence conditions we use the function

$$r(z)=(1-\chi_{\min})e^{-0.5(z/z_0)^2}+\chi_{\min}. \tag{6}$$

Its shape resembles the depth dependence of the hitting probability for ion backscattering under channeling incidence conditions [38]. The parameter z_0 in Eq. (6) is varied until good agreement between the simulated and the measured random spectra above 1.75 keV—where there is in both random and aligned cases no Auger contribution—is obtained. The value for $\chi_{\min}$ is taken from the ion backscattering data; see Table I. We define the integral of $r(z)-\chi_{\min}/2$ from $z=0$ to 100 Å as the effective layer thickness L_B for the generation of background electrons under channeling incidence conditions. This procedure is comparable to that applied for the evaluation of the surface peak area in ISS [38]. It is noted that Kudo *et al.* [21,22] use a similar quantity, *effective target thickness*, which they apply to both the aligned and the random spectra.

We find best results for an effective layer thickness L_B of 33 (±3) Å and for $\gamma=-6.3$ (±0.2); see Tables II and III. The fitted random and aligned background spectra are shown as the full curves in Fig. 1. Their slopes in the double-log plot are -5.1 ± 0.2 ($=\alpha_r$) and -6.0 ± 0.2 ($=\alpha_a$), respectively. As predicted by Eqs. (3) and (4), α_r differs by about +1 from γ, while $\alpha_a\sim\gamma$. We see in Fig. 1 that the fitted random background spectrum approaches but does not intersect the measured random spectrum near 1.0 keV, far below the *KLL* and *KLM* Auger transition energies. This observation shows that it is possible to extrapolate the *random* background spectrum from the high (>1.75 keV) energy region over many hundreds of eV with the help of the *aligned* background spectrum plus the Monte Carlo simulations. To summarize: The aligned spectrum is used to obtain a good estimate for the initial energy distribution, while the Monte Carlo model is used to obtain a good estimate for the final (or detected) energy distribution under random incidence conditions.

An identical analysis is applied to the Al data. The results are summarized in Tables II and III also. Considering the approximations, it is surprising that the values for L_B according to the SL-CSDA model are in such good agreement with the Monte Carlo results.

C. Monte Carlo simulations of the *KLL-KLM* Auger spectra

After subtraction of the fitted background from the measured spectra, the residual *KLL-KLM* Auger electron spectra are obtained. They are shown in Figs. 2 and 3 for Si and Al, respectively. The error bars in Fig. 2 at 1.1, 1.3, and 1.5 keV indicate the uncertainty in the method of background subtraction. Using the Monte Carlo model we have simulated the shape of the Auger spectra too. The energy positions are from Ref. [27], and the relative strengths of the various Auger peaks are the same as in Refs. [16,18]. If spectrum shifts and broadening due to multiple ionization are neglected, the simulated aligned Auger spectra consist of three narrow peaks with small, slowly decaying tails on the low-energy side [23]. The tails are caused either by the few electrons generated far below the surface ($z\gg L_A$) or by those electrons generated near the surface but emitted inward and at some finite depth scattered back toward the surface. These simulated Auger spectra do not agree with the measured spectra, which we attribute to the effects of multiple ionization. In order to include these effects, the simulated Auger spectra are convoluted with a function $g(E')$ representing the shift and broadening of the initial energy distribution of the Auger electrons. In Refs. [18,23] we have modeled $g(E')$ via

$$g(E')=\begin{cases}\dfrac{\kappa}{\mu+\nu\kappa}\,e^{(E'+\mu)/\nu} & \text{for } E'<-\mu,\\ \dfrac{1}{\mu+\nu\kappa} & \text{for } -\mu<E'<0,\\ 0 & \text{for } E'>0,\end{cases} \tag{7}$$

where κ, μ, and ν are three parameters and $E'\equiv E-E_A$; E_A is the undisturbed (i.e., characteristic) Auger transition energy. The choice for this particular function $g(E')$ is based on data from Refs. [30,31]. The region where $-\mu<E'<0$ corresponds roughly to multiple *KM* ionization, while the region where $E'<-\mu$ corresponds roughly to multiple *KL* ionization.

We have fitted the convoluted simulated Auger spectra to the experimental ones. The fitting parameters are κ, μ, ν, z_0, and a general scaling parameter. Aligned and random spectra are fitted simultaneously. For the Si Auger spectra, the fit yielded for κ, μ, and ν: 0.60, 40 eV, and 22 eV, respectively; and for the Al spectra: 0.65, 16 eV, and 30 eV, respectively. The fitted Auger spectra are shown by the full curves in Figs. 2 and 3. The corresponding results for the effective layer thickness L_A for the generation of *KLL* Auger electrons under channeling incidence conditions are summarized in Table II, fifth column. Note that L_A turns out to be always smaller than L_B. The values for κ, μ, and ν follow mainly from the aligned Auger spectra, while the value for L_A follows from the comparison between the aligned and the random Auger spectra. We note that the results for κ, μ, and ν are mutually interdependent; e.g., a decrease in μ and an increase in κ produce fits that are almost as good. One sees that the simulated random Auger spectra follow the measured ones

closely down to an energy of at least 400 eV below the main Auger transition energy. At lower energies, the measured Auger spectra often fall below the simulated ones, probably because of the increased error in the subtracted background.

IV. DISCUSSION

The effect of ion channeling on secondary electron emission (SEE) has been studied by Kudo *et al.* [21,22]. For the case of 6 MeV/u protons and deuterons along the Si [110] axis [22], these authors observed an aligned-to-random SEE ratio of ~0.35. In our case, we found a value of 0.21 (Table I). We attribute this difference to the high energy of the ion beam in Kudo's experiments. First, the shadowing effect in the outermost atomic layers is less pronounced for higher beam energies [38]. Second, although the authors have determined the aligned-to-random ratio at ~8 keV, the binary-encounter energy E_B is so high (13 keV) that also the less localized outer-shell electrons contribute substantially to SEE. We note furthermore that α_r in their spectra is about -4.5 at 8 keV. The effect of ion channeling on the intensity of the *derivative* ion-induced Auger electron signal has been explained quantitatively by MacDonald *et al.* [19,20]. In their analysis, however, the information on electron-transport properties contained in the remaining part of the spectrum is lost.

A. Shape of the background spectra

Under channeling incidence conditions, the Auger electron contribution to the measured secondary electron spectrum is limited to a range of about 250 eV below the main Auger transition energy. The remaining part of the spectrum can be attributed almost exclusively to background electrons, i.e., electrons emitted by direct Coulomb ionization. The fitted random and aligned background spectra are well described by a power-law function: $Y_B(E) \propto E^{\alpha}$. The average exponent α in all (Si and Al) random spectra differs by $+0.7\pm0.2$ from the average exponent in all aligned spectra: $\langle\alpha_r\rangle=-5.15\pm0.10$ and $\langle\alpha_a\rangle=-5.85\pm0.20$; see Table II. The simple straight-line and continuous-slowing-down (SL-CSDA) model predicts a difference of $+1$. However, the underlying assumption that for channeling incidence all secondary electrons are produced in a very thin surface layer is of course not strictly valid. The successful Monte Carlo analysis reveals that not only the aligned and random background spectra but also the initial energy distribution $f(E)$ of the background electrons are well described by a power-law function: $f(E) \propto E^{\gamma}$. For the three different geometries studied and for Si and Al alike, we obtain within ±0.2 the same value for γ: -6.3. It is noted that there is a systematic uncertainty of ±0.5 in γ due to the uncertainty in the energy dependence of the electron analyzer sensitivity function. We see that on the average $\alpha_r-\gamma=1.2\pm0.2$, consistent with the simple SL-CSDA model.

Folkmann *et al.* [39] have measured the shape of continuous-energy spectra of electrons emitted from solid carbon targets under bombardment by (0.5–10)-MeV H^+ and Ne^+ ions. They compared experimental data with binary-encounter-approximation calculations. For electron energies above E_B, both their measured and calculated intensities exhibit a power-law behavior with an exponent of about -8, not inconsistent with our results.

B. Shape of the Auger electron spectra

In Refs. [16,18] we have applied an analytical model for electron transport in matter to analyze ion-induced Al and Si *KLL-KLM* Auger electron spectra. The rather simple model—but also more elaborate models [2,5,40]—predicts a spectral intensity that is constant for small energy losses ΔE and decreases proportional to $\Delta E^{-1/2}$ for larger losses. Although the model spectra agreed qualitatively with the measured spectra, the spectrum range of constant intensity was much too narrow, i.e., about 50 eV instead of 700 eV. In the present work we find good agreement between the measured spectra and spectra calculated with the Monte Carlo simulation model. Only at low energies (ΔE>400 eV) do the simulated random Auger spectra tend to be more intense than the measured ones, probably because of the inaccuracy in the method of background subtraction.

The intensity of the aligned Auger spectra decreases rapidly with decreasing electron energy. It is, of course, a consequence of the relatively low number of electrons generated deep within the solid. But also in the random case, there is a decrease in intensity, although less pronounced. There are several causes for this decrease. First, the stopping power increases with decreasing electron energy, causing a gradual decrease in spectrum intensity. Second, as discussed in the beginning of Sec. III, the average path length of the electrons in the specimen before escape increases faster than linearly with generation depth because of elastic scattering. This leads to larger energy losses and, thus, to a lower intensity at lower energies. However, since the cross section for elastic scattering is relatively small, the effect of the increased path length is modest. Surprisingly, the most prominent cause for the decrease in spectrum intensity below E_A is the discrete character of the energy-loss mechanism [23]. Of particular importance are the energy-loss events larger than ~100 eV, i.e., losses by L-shell ionization. They are relatively rare; the mean free path λ_i^* is ~200 Å, while for all losses combined λ_i is only ~30 Å. Nevertheless, a large energy loss is involved. Consequently, their contribution to the stopping power is non-negligible, indeed about 40% for (1–2)-keV electrons in Al or Si. For generation not far below the surface ($z \ll \lambda_i^*$), the L-shell contribution to the average energy loss per angstrom is absent for most detected electrons. Hence, the spectrum intensity is approximately inversely proportional to the *reduced* stopping power, i.e., the stopping power without the L-shell contribution. With increasing generation depth, increasingly more electrons will have experienced at least one large (>100 eV) energy loss event before escape; the L-shell contribution to the stopping power becomes increasingly more important. Consequently, the spectrum intensity decreases to a level inversely proportional to the *full* stopping power. Note that the decrease in the spectra of Figs. 2 and 3 is partly obscured by the interference among the three Auger peaks. It is mainly because this (apparent) reduced stopping power effect is discarded in the analytical model used in Refs. [16,18] that it was then not possible to find agreement between measured and calculated spectra.

Needless to say, the Monte Carlo model automatically incorporates this (apparent) reduced stopping power effect.

C. Effective layer thickness for SEE under channeling incidence

Both ion backscattering and the generation of electrons by inner-shell ionization can occur only when the ion approaches the atomic nucleus within a very small distance. For ion backscattering, the distance is the collision diameter, $r_c = 2Z_1Z_2e^2/E_p$; and for inner-shell ionization, it is the adiabatic radius, $r_{\rm ad} = \hbar v/U$, where v is the ion velocity and U is the ionization energy. In our experiments, $r_c \sim 0.06$ pm, $r_{\rm ad}$(K shell) ~3 pm, and $r_{\rm ad}$(L shell) ~50 pm (1 pm$=10^{-12}$ m). The former two distances are smaller than the two-dimensional vibration amplitude (ρ) for atoms in the bulk: 11 pm for Si and 16 pm for Al [41]. Therefore, one expects that the probability for Al or Si K-shell ionization is affected by channeling in the same manner as the probability for ion backscattering, i.e., decreasing in the same manner with depth. Using a (very distinct) Monte Carlo model for ion channeling [42], we have calculated the effective layer thickness $L_{\rm ISS}$ for ion backscattering and L_K for K-shell ionization. Note that in most ion scattering work $L_{\rm ISS}$ is called the surface peak area. In these calculations, the structures of the (2×1) reconstructed Si(100) surface [43] and of the relaxed Al(110) surface [44] have been used. The assumed enhancements in ρ for first- and second-layer atoms are 40% and 20%, respectively. The theoretical results for $L_{\rm ISS}$ and L_K are given in the last two columns of Table II. Note that, because of the finite values of $r_{\rm ad}$, the theoretical effective layer thickness for K-shell ionization is slightly larger than that for ion backscattering.

For ion backscattering from Al, the experimental values of $L_{\rm ISS}$ agree with the theoretical values. For Si, there is a discrepancy, but the value cited has been determined in an indirect way—by comparison with another experiment—and is, therefore, not fully reliable. However, it must be noted that also in Ref. [18] a discrepancy has been observed. For Si, the experimental value for L_A (KLL Auger electron generation) and the theoretical value for L_K (K-shell ionization) are in agreement with each other. For Al, the experimental values are 21±10 % larger. The outcome of a determination of L_A depends on the value of the stopping power. The successful comparison between theory and experiment justifies the value for the Si stopping power: 1.6±0.2 eV/Å for 1.6-keV electrons [32]. In order to obtain good agreement also for the Al data, we must assume an Al stopping power at 1.4 keV of 2.5±0.2 eV/Å instead of 2.1 eV/Å [32].

The experimental values for the effective layer thickness L_B for the background electrons are on the average 1.8 (±0.2) times larger than the values for L_K. Obviously, this difference must be related to the mechanism of secondary electron generation. An extensive review of electron production in ion-atom collisions is given by Rudd and Macek [45]. Classically, the maximum energy transfer of a 1.5-MeV He^+ ion to a free electron at rest is 0.81 keV ($=E_B$). However, because K- and L-shell electrons are initially not at rest, the emitted electrons can have energies far above E_B. Assuming that the bound electrons have a fixed kinetic energy equal to U, Thomas derived classically [46] a maximum energy transfer of $E_B + 2\sqrt{E_B U}$. For the Al and Si L shell, this amounts to ~1.4 keV; and for the K shell, ~3.2 keV. Furthermore, the interaction time Δt of the ion with the electrons is of the order of a_n/v, in which a_n is the shell radius. Because of quantum-mechanical considerations, the finite interaction time implies a finite uncertainty in the energy ΔE of the ejected electrons: $\Delta E = \hbar/\Delta t = \hbar v/a_n$. For the Si and Al K shell, $\Delta E \sim 1.4$ keV; and for the L shell, $\Delta E \sim 0.3$ keV. Therefore, the intensity of secondary electrons above $E_B + 2\sqrt{E_B U}$ is not zero but finite. The upper limit ($\sim E_B + 2\sqrt{E_B U} + \hbar v/a_n$) is about 4.8 keV for the K shell and 1.7 keV for the L shell. Thus, we conclude that the observed large values for L_B are due to the non-negligible contribution from the less localized L shell. We must note here that in our analysis we have assumed that L_B is constant for the energy range studied (1–2 keV). In fact, this cannot be fully correct because the relative L-shell contribution varies with energy. The energy dependence of L- and K-shell SEE is the subject of a forthcoming study.

A complication in comparing experiment and theory is the anisotropy in the intensity of the secondary electrons [47]. The Monte Carlo model assumes isotropic emission. This negligence is, however, not very serious because all analyses are based upon a comparison between aligned and random spectra. Another complication is the crystalline structure of the solid. In electron-induced AES, large directional variations in the intensity have been observed; see, e.g., Ref. [48]. The main source for these variations is, according to most authors, diffraction of the incident electron beam, and thus is irrelevant in our experiments. Using angle-resolved XPS, where effects of the incident beam are absent, Hill *et al.* [49] observed that for some exit directions, the intensity of Si photoelectrons was ~20% higher than average. Egelhoff [50] measured variations of ~40% for angle-resolved XPS of Cu. In general, diffraction and focusing by the attractive Coulomb potential of the atomic rows are believed to be the main cause of these variations [51]. As a consequence of our experimental setup, alignment of the incident beam with a major crystallographic direction implies always (near) alignment of the analyzer with some crystallographic direction; e.g., for incidence along the [011] direction of the Al(110) crystal, the analyzer is oriented close to the $[2\bar{1}1]$ direction. Therefore, the aligned secondary electron intensities may have been affected by the crystalline structure of the specimen. We estimate that in our experiments this effect is at most 20%. Note that also this effect could explain the 20% discrepancy between the experimental and theoretical effective layer thicknesses for K-shell ionization in Al.

V. SUMMARY AND CONCLUSIONS

Spectra in the (1–2)-keV range of secondary electrons induced by channeled and nonchanneled 1.5-MeV He^+ ions have been measured. The specimens studied are Si(100) and Al(110). Both the spectra of the background electrons, generated by direct Coulomb ionization, and of the Auger electrons are analyzed by using an efficient Monte Carlo simulation model for electron transport. This model faithfully reproduces the aligned and random KLL Auger spectra and explains the apparent discrepancies found in Refs. [16,18], where an analytical model by Tougaard and Sigmund [2] was

applied. Our work shows that the decrease in random Auger spectrum intensity down to 300 eV below the characteristic Auger energy E_A is a consequence of the large (>100 eV) energy-loss events. Analysis of the background spectrum shows that the initial energy distribution of the background electrons varies with electron energy as $E^{-6.3\pm0.5}$ above the binary-encounter energy E_B.

In the case of ion channeling, an effective layer thickness L for inner-shell ionization can be defined. This quantity is related to the surface peak area L_{ISS} for high-energy ion backscattering. In the present work, quantitative analysis of the Al and Si KLL Auger electron spectra—i.e., measurement of L_{Auger}—is only possible by means of the Monte Carlo model. We find that $L_{\mathrm{Auger}}=L_{\mathrm{ISS}}$, while $L_{\mathrm{background}}>L_{\mathrm{ISS}}$. In other words, the generation of background electrons is less affected by ion channeling than the generation of KLL Auger electrons. This difference is attributed to the relatively large contribution to the secondary electron spectra from the Al and Si L shell, also at energies well above E_B.

To conclude, MeV ion-induced electron emission in combination with ion channeling offers unique opportunities to study the generation and transport of energetic electrons in solids. For instance, electron transport models can be tested, the stopping power for electrons can be measured, and the mechanism for high-energy secondary electron generation can be studied. Furthermore, improved understanding of the Auger peak shape is particularly useful for quantification of conventional—i.e., electron-induced—AES or of XPS, as we have shown in Refs. [24,25].

ACKNOWLEDGMENTS

The authors are grateful for the support of J. R. MacDonald (University of Guelph) and of the Natural Science and Engineering Research Council of Canada throughout the course of these studies, and for the helpful discussion with P. A. Zeijlmans van Emmichoven (Utrecht University).

[1] C. J. Powell, J. Vac. Sci. Technol. A **4**, 1532 (1986).

[2] S. Tougaard and P. Sigmund, Phys. Rev. B **25**, 4452 (1982).

[3] R. Bindi, H. Lanteri, and P. Rostaing, Surf. Sci. **197**, 295 (1988).

[4] A. L. Tofterup, Surf. Sci. **227**, 157 (1990); **248**, 77 (1991).

[5] V. M. Dwyer and J. M. Richards, Surf. Interface Anal. **20**, 271 (1993).

[6] I. S. Tilinin and W. S. M. Werner, Surf. Sci. **290**, 119 (1993).

[7] A. Jablonski, Surf. Sci. **188**, 164 (1987).

[8] Z.-J. Ding and R. Shimizu, Surf. Sci. **197**, 539 (1988).

[9] J. Luis del Barco and J. Ferron, Surf. Sci. **232**, 393 (1990).

[10] W. S. M. Werner, Surf. Interface Anal. **18**, 217 (1992).

[11] H. Yoshikawa, T. Tsukamoto, R. Shimizu, and V. Crist, Surf. Interface Anal. **18**, 757 (1992).

[12] P. J. Cumpson, Surf. Interface Anal. **20**, 727 (1993).

[13] K. O. Jensen and A. B. Walker, Surf. Sci. **292**, 83 (1993).

[14] J. D. Martinez, R. Mayol, and F. Salvat, J. Appl. Phys. **67**, 2955 (1990).

[15] N. Öztürk and W. Williamson, Jr., J. Appl. Phys. **74**, 4723 (1993).

[16] L. Wong, P. F. A. Alkemade, W. N. Lennard, and I. V. Mitchell, Nucl. Instrum. Methods B **45**, 637 (1990).

[17] P. F. A. Alkemade, L. Wong, W. N. Lennard, and I. V. Mitchell, Nucl. Instrum. Methods B **48**, 604 (1990).

[18] P. F. A. Alkemade, W. N. Lennard, and I. V. Mitchell, Surf. Sci. **248**, 173 (1991).

[19] J. R. MacDonald, L. C. Feldman, P. J. Silverman, J. A. Davies, K. Griffiths, T. E. Jackman, P. R. Norton, and W. N. Unertl, Nucl. Instrum. Methods **218**, 765 (1983).

[20] J. R. MacDonald, L. C. Feldman, P. J. Silverman, J. A. Davies, and T. E. Jackman, Surf. Sci. **157**, L335 (1985).

[21] H. Kudo, K. Shima, S. Seki, and T. Ishihara, Phys. Rev. B **43**, 12 736 (1991); H. Kudo, K. Shima, K. Masuda, and S. Seki, *ibid.* **43**, 12 729 (1991).

[22] H. Kudo, K. Shima, and T. Ishihara, Phys. Rev. B **47**, 27 (1993).

[23] P. F. A. Alkemade, W. N. Lennard, and I. V. Mitchell, in *Interaction of Charged Particles with Solids and Surfaces*, edited by A. Gras-Marti *et al.* (Plenum, New York, 1991), p. 599.

[24] P. F. A. Alkemade, K. Werner, S. Radelaar, and W. G. Sloof, Appl. Surf. Sci. **70/71**, 24 (1993).

[25] P. F. A. Alkemade, Surf. Interface Anal. **23**, 451 (1995).

[26] J. A. Davies, T. E. Jackman, H. L. Eschbach, W. Dobma, U. Wätjen, and D. Chivers, Nucl. Instrum. Methods B **15**, 238 (1986), and references therein.

[27] L. E. Davis, N. C. MacDonald, P. W. Palmberg, G. E. Riach, and R. E. Weber, *Handbook of Auger Electron Spectroscopy*, 2nd ed. (Physical Electronics Industries, Eden Prairie, 1976).

[28] P. Richard, R. L. Kauffman, J. H. McGuire, C. F. Moore, and D. K. Olsen, Phys. Rev. A **8**, 1369 (1973).

[29] W. Schmidt, P. Müller, V. Brückner, F. Löffler, G. Saemann-Ischenko, and W. Schubert, Phys. Rev. A **24**, 2420 (1981).

[30] M. O. Krause, in *Atomic Inner Shell Processes*, edited by B. Crasemann (Academic, New York, 1975), Vol. 2, p. 65.

[31] A. K. Edwards and M. E. Rudd, Phys. Rev. **170**, 140 (1968).

[32] C. J. Tung, J. C. Ashley, and R. H. Ritchie, Surf. Sci. **81**, 427 (1979).

[33] J. Lindhard, K. Dan. Vidensk. Selsk. Mat. Fys. Medd. **28**, 3 (1954).

[34] M. Fink and J. Ingram, At. Data **4**, 129 (1972).

[35] D. Gregory and M. Fink, At. Data Nucl. Data Tables **14**, 39 (1974).

[36] M. E. Riley, C. J. MacCallum, and F. Biggs, At. Data Nucl. Data Tables **15**, 443 (1975).

[37] E. N. Sickafus, Phys. Rev. B **16**, 1436 (1977).

[38] See, e.g., I. Stensgaard, L. C. Feldman, and P. J. Silverman, Surf. Sci. **77**, 513 (1978).

[39] F. Folkmann, K. O. Groeneveld, R. Mann, G. Nolte, S. Schumann, and R. Spohr, Z. Phys. A **275**, 229 (1975).

[40] V. M. Dwyer and J. A. D. Matthew, Surf. Sci. **193**, 549 (1988).

[41] D. S. Gemmel, Rev. Mod. Phys. **46**, 129 (1974).

[42] J. W. M. Frenken, R. M. Tromp, and J. F. van der Veen, Nucl.

Instrum. Methods B **17**, 334 (1986).
[43] R. M. Tromp, R. G. Smeenk, F. W. Saris, and D. J. Chadi, Surf. Sci. **133**, 137 (1983).
[44] J. N. Andersen, H. B. Nielsen, L. Petersen, and D. L. Adams, J. Phys. C **17**, 173 (1984).
[45] M. E. Rudd and J. H. Macek, in *Case Studies in Atomic Physics*, edited by E. W. McDaniel and M. R. C. McDowell (North-Holland, Amsterdam, 1974), Vol. 3, p. 47.
[46] L. H. Thomas, Proc. Cambridge Philos. Soc. **23**, 713 (1927).
[47] N. M. Kabachnik, in *Electronic and Atomic Collisions*, edited by H. B. Gilbody, W. R. Newell, F. H. Read, and A. C. H. Smith (North-Holland, Amsterdam, 1988), p. 221.
[48] H. E. Bishop, B. Chornik, C. LeGressus, and A. LeMoel, Surf. Interface Anal. **6**, 116 (1984).
[49] J. M. Hill, D. G. Royce, C. S. Fadley, L. F. Wagner, and F. J. Grunthaner, Chem. Phys. Lett. **44**, 225 (1976).
[50] W. F. Egelhoff, Jr., Phys. Rev. Lett. **59**, 559 (1987).
[51] H. C. Poon and S. Y. Tong, Phys. Rev. B **30**, 6211 (1984).